33RD INTERNATIONAL COSMIC RAY CONFERENCE, RIO DE JANEIRO 2013
THE ASTROPARTICLE PHYSICS CONFERENCE

The EVA code: Macroscopic modeling of radio emission from air showers

KRIJN D. DE VRIES[1], OLAF SCHOLTEN[2], KLAUS WERNER[3],

[1] *Vrije Universiteit Brussel (VUB), dienst ELEM, Pleinlaan 2, B-1050 Brussels, Belgium*
[2] *Kernfysisch Versneller Instituut, University of Groningen, 9747 AA, Groningen, The Netherlands*
[3] *SUBATECH, University of Nantes – IN2P3/CNRS– EMN, Nantes, France*

krijndevries@gmail.com

Abstract: We discuss the EVA code which is based on a macroscopic approach to calculate radio emission from air showers. Recently it was shown that Cherenkov effects play a crucial role in the emission. The advantage of the macroscopic approach is that it allows for resolving the divergences in the electric field expressions due to these Cherenkov effects, which is done by using the finite extent of the particle distribution in the shower front. Furthermore, the macroscopic approach allows for a more intuitive interpretation of the observed radio-emission pattern in terms of the properties of the air shower such as the longitudinal profile and the thickness of the shower front. The particle distributions and currents in the air shower front are obtained in histograms from a full CONEX Monte-Carlo air shower simulation. A fitting procedure is applied to obtain smooth analytic functions which are used to solve for the radio emission including Cherenkov effects. The EVA code is publicly available.

Keywords: Radio emission, Cosmic ray air showers, Shower simulations, Index of refraction, Geomagnetic Cherenkov radiation

1 Introduction

In recent years much progress has been made in the modeling of radio emission from cosmic-ray-induced air showers. This progress was initiated by the successful CODALEMA [1, 2] and LOPES [3, 4] experiments, showing the feasibility of radio emission as a detection mechanism for air showers. These results triggered plans for new experiments such as AERA [5] at the Pierre Auger Observatory, LOFAR [6], and the TUNKA-REX [7] experiment. Along with these new initiatives came the need for more detailed models describing the radio emission. Several radio emission models were developed such as REAS [8] and MGMR [9], and more recently CoREAS [10], ZHAires [11], SELFAS [12], Kalmyakov *et al.* [13] and the EVA code [14].

Even though there have been several new modeling attempts since the beginning of the 21'st century, the observed radio emission mechanisms were already predicted in the 1960's. Kahn and Lerche [15] predicted the geomagnetic emission mechanism due to the separation of electrons and positrons by Earth's magnetic field. At the same time Askaryan [16] predicted the emission by the net negative electron excess in the shower front mainly due to Compton scattering. The geomagnetic emission mechanism is already observed by CODALEMA [2] and LOPES [17], and more recently signatures of the charge-excess emission have been observed at the Pierre Auger Observatory [18] and CODALEMA [19].

The latest theoretical development is the inclusion of Cherenkov effects in the radio emission [20] leading to divergences in the electric field expressions. The EVA model uses the finite extent of the charge and current distributions in the shower front to solve for these divergences. The distributions are obtained from a full Monte-Carlo CONEX [21, 22] simulation. Accordingly, these distributions are fitted to obtain smooth analytical expressions which are used to solve for the divergences in the electric field expressions. In these proceedings, first we give a short introduction to the EVA-model, after which we discuss the charge and current distributions in the shower front. Finally, we discuss the obtained radio pulse and how the emission is affected by Cherenkov effects. For a more detailed discussion of the applications of Cherenkov effects and how to separate the different radio emission mechanisms we refer to [23].

2 The model

The EVA model is based on the macroscopic current and particle distributions in the shower front. Following [14], the point-like Liénard-Wiechert potentials at the observer time t and observer position $\vec{x}$ can be defined as,

$$A^{\mu}_{PL}(t,\vec{x}) = \frac{\mu_0}{4\pi}\frac{J^{\mu}_{PL}}{|\tilde{R}V|}|_{t=t'}, \tag{1}$$

where the point-like four current J^{μ}_{PL} is given by,

$$J^{\mu}_{PL}(t',\vec{x}) = J^{\mu}(t')\delta^3(\vec{x}-\vec{\xi}(t')). \tag{2}$$

Here $\vec{\xi}(t') = -ct'\vec{e}_{x^{||}}$ gives the position of the shower front along the shower axis at the negative retarded emission time t'. The four-distance $\tilde{R}$ is defined by its scalar component $\tilde{R}^0 = L = c(t-t')$, where L is given by the optical path length from the emission point to the observer, and the spatial components $R^i = -L\frac{\partial}{\partial\xi^i}L$. The velocity of the shower is defined by, $V = c^{-1}d\xi/dt'$.

2.1 Cherenkov effects

In [24] it was shown that, even though the refractivity in air deviates only slightly from zero ($O(10^{-4})$), this leads to Cherenkov effects in the radio emission from air showers. An intuitive way of understanding these Cherenkov effects is by having a closer look at the denominator in Eq. 1. In [24] it is shown that this denominator scales with the

derivative of the observer time with respect to the emission time $\tilde{R}V \propto dt/dt'$. In Fig. 1, the emission height $z = -\beta c t'$

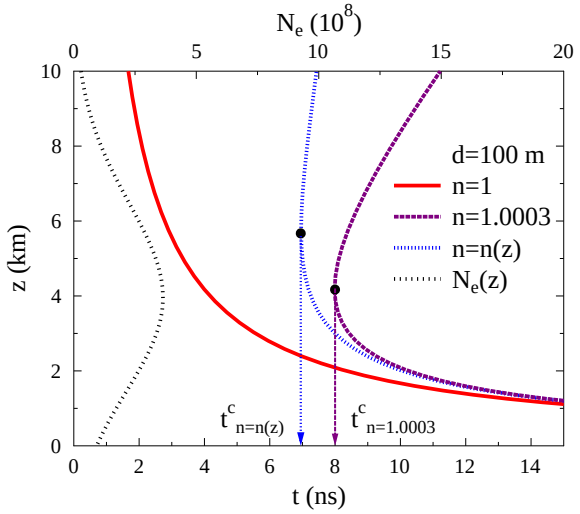

Figure 1: The emission height $z = -\beta c t'$ as function of the observer time t for three different values of the index of refraction, n. The dashed black line gives the shower profile as function of z for a $E = 5 \times 10^{17}$ eV proton-induced shower.

is plotted as a function of the observer time for three different values of the index of refraction n. This is done for a horizontal incoming shower of 5×10^{17} eV with the observer positioned at $d = 100$ m from the shower axis. For an index of refraction equal to its vacuum value of unity the signal will travel with the same speed as the shower. Signals emitted at a large height move in a straight line toward the observer, whereas signals emitted at lower heights first "travel" along with the shower and then move in a straight line toward the observer. Therefore, signals emitted at a lower height effectively have to "travel" a larger distance and will arrive at later times. This is shown by the solid red line in Fig. 1, which is a constant decreasing function of the observer time and hence the denominator $\tilde{R}V \propto dt/dt'$ is finite at all observer times.

What happens if we take an index of refraction equal to its value at sea level, $n = 1.0003$? Due to this small deviation of the index of refraction from unity, the signal will travel slightly slower than the shower which moves at the vacuum speed of light. Therefore, even though signals emitted from a lower height have to "travel" a net larger distance, since they first travel along with the shower (moving with the vacuum speed of light), their average speed will be larger than the average speed of a signal which is emitted at large heights traveling straight toward the observer. As a consequence signals emitted from large heights can arrive at exactly the same time as signals emitted at a later stage of the shower development. There will also be a "critical" height where all signals emitted slightly above or slightly below this height will be projected instantly toward the observer and hence the observed radio signal is strongly enhanced. This is the Cherenkov effect. At this point the denominator $\tilde{R}V \propto dt/dt'$ vanishes and the vector potential hits a singularity. This is observed for the dashed purple line in Fig. 1. From this figure it also follows that the starting time of the radio emission corresponds to the time at which Cherenkov effects are observed.

In reality the index of refraction will depend on the air density and thus the observer height. The EVA code models the index of refraction following the Gladstone-Dale law,

$$n_{\rm GD} = 1 + 0.266 \frac{\rm cm^3}{\rm g} \rho(z). \qquad (3)$$

The emission height as function of the observer time is given by the striped blue line in Fig. 1 in this realistic situation. As expected the line lies in between the lines for a vacuum index of refraction (solid red line) and a constant index of refraction equal to its value at sea level (dashed purple line). As a reference, in Fig. 1 we also plot the total number of particles as a function of emission height (striped black line). It follows that for the specific geometry shown in Fig. 1, Cherenkov effects are observed from the shower maximum and are thus expected to play a crucial role in the emission.

2.2 The electric fields; Solving for the divergences

The electric field is obtained from the Liénard-Wiechert potentials using the standard relation,

$$E^i = -c\left(\partial^0 A^i + \partial^i A^0\right). \qquad (4)$$

Since the denominator in the vector potential in general is a function of position and time $\tilde{R}V(\vec{x},t)$, the electric field will scale like $E \propto \frac{1}{(\tilde{R}V)^2}$ leading to a bad divergence when Cherenkov effects are observed in the emission. To solve for these divergences, we make use of the finite extend of the shower front described by the weight function $w(\vec{r},h)$, where $\vec{r}$ gives the lateral position in the shower front and h the longitudinal position. The complete vector potential can now be written as a convolution of the weight function and the point-like vector potential,

$$A^\mu(\vec{x},t) = \int d\vec{r} \int dh\, w(\vec{r},h) A^\mu_{PL}(\vec{\xi} - \vec{x}, t). \qquad (5)$$

At this point we apply a coordinate transformation defining $\vec{\eta}^{\perp i} = \vec{x}^{\perp i} + \vec{r}$ for the transverse components and $\lambda = h_k - h$ in the longitudinal direction. Where h_k is the critical value for h where the denominator $\tilde{R}V(h_k) = 0$. By this shift in coordinates it can be shown [14], that the derivatives acting on the denominator of the vector potential vanish independently. The total electric field is now given by,

$$\begin{aligned} E^{||} &= -c \int d^2\eta^\perp \int_0^{h_k} d\lambda \\ &\quad \left\{ w' A^0_{PL} - \beta w' A^{||} + w \dot{A}^{||}_{PL} \right\} \\ E^{\perp i} &= c \int d^2\eta^\perp \int_0^{h_k} d\lambda \\ &\quad \left\{ w^i A^0_{PL} + \beta w' A^{\perp i}_{PL} - \beta w \dot{A}^{\perp i}_{PL} \right\}, \end{aligned} \qquad (6)$$

separating the longitudinal component of the electric field $E^{||}$ and the lateral components $E^{\perp i}$ (i=1,2). The derivatives of the weight functions are given by $w' = dw/dh$, and $w^i = dw/dx^i$. The derivatives acting on the potentials are denoted by $\dot{A} = dA/d(ct)$. The remaining square root divergence in the vector potential is now safely integrated.

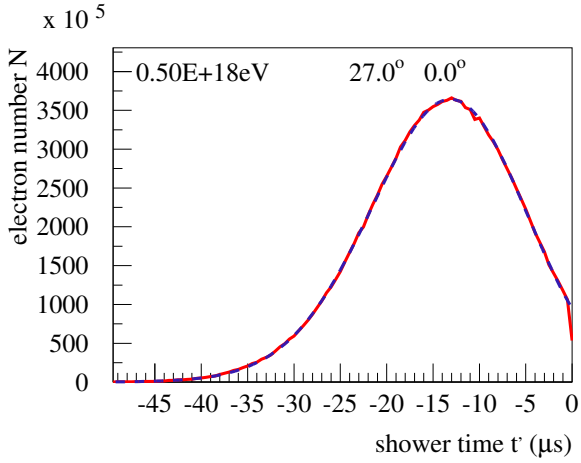

Figure 2: The number N of electrons and positrons, as a function of the shower time t' The full red line represents the simulation result, the dashed blue line is the fit. Figure taken from [14].

3 The EVA package

The EVA package consists out of three different parts,

- The CX-MC-GEO air shower simulation package
- The FITMC package
- The EVA radio emission calculation package

The CX-MC-GEO package is a full Monte-Carlo CONEX [21, 22] air shower simulation providing histograms of the relevant charge and current distributions in the air shower. These histograms are fitted to smooth analytic functions by the FITMC package. The EVA radio emission calculation package uses the obtained fit function from FITMC to solve numerically for the electric fields.

Coherence in the radio emission is determined by the largest projected length scale toward the observer [25]. An observer positioned far away from the shower axis will see the shower front in a single point, and hence coherence is determined by the projected shower profile. Observers positioned at distances where Cherenkov effects occur, observe signals emitted at different stages of the shower development instantaneously. Therefore, in this regime coherence is determined by the particle distributions in the shower front. To understand the consequences of Cherenkov effects in radio emission from air showers, it is thus crucial to have a proper description of the shower profile and the particle distributions in the shower front. In Fig. 3 we show the shower profile as obtained by CX-MC-GEO (red solid line) and the fit obtained by FITMC (blue dashed line), giving an excellent fit. The particle distribution in the shower front is assumed to be radially symmetric and separated in two functions,

$$w(r,h) = 2\pi r\, w(\vec{r},h) \quad (7)$$

$$w(r,h) = w_1(r) w_2(r,h), \quad (8)$$

where $w_1(r)$ describes the radial weight function and $w_2(r,h)$ the longitudinal weight function which will depend on the radial distance r from the shower axis. Coherence is mainly determined by the longitudinal weight function.

The weight functions are fitted by two different functions for radial distances $r < 20$ m and $r > 20$ m. Fits to the longitudinal distributions at $r = 5$ m and $r = 128$ m from the shower axis are given in Figs. 3 and 4. It follows that close to the shower axis this distribution becomes very narrow leading to coherence at very high frequencies in the emission. More details about the fits are given in [14] where it is also shown that the lateral weight function, $w_1(r)$, peaks close to the shower axis.

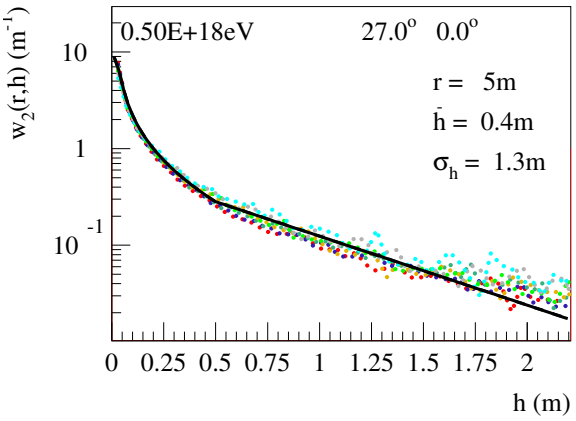

Figure 3: The distribution $w_2(r,h)$ for $r = 5$ m. The full black line represents the fit, the dotted lines are simulation results for different times. Figure taken from [14].

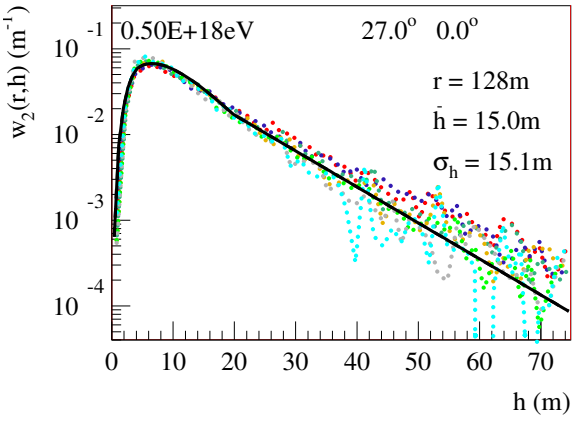

Figure 4: The distribution $w_2(r,h)$ for $r = 128$ m. The full black line represents the fit, the dotted lines are simulation results for different times. Figure taken from [14].

Nevertheless, there is one caveat, which is the current distribution in the shower front. Recent simulations indicate that the geomagnetic current as well as the charge-excess current increase with distance from the shower axis. This is also shown in Fig. 5, where we plot the geomagnetically induced drift velocity given by $v_d = J^x/Nec$ as a function of radial distance from the shower axis. The radial dependence of the currents in the shower front is implemented in the latest version of EVA1.03.

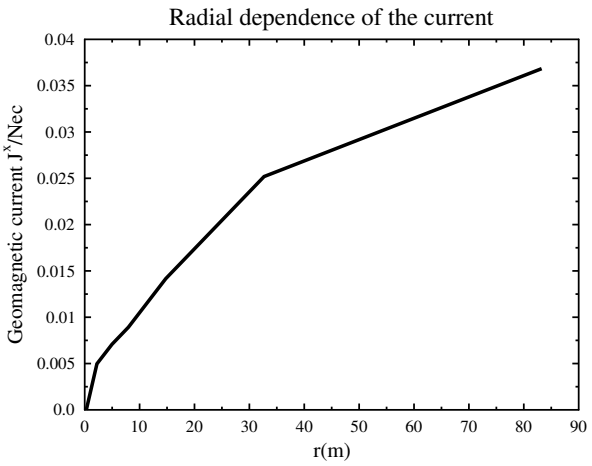

Figure 5: The geomagnetically induced drift velocity as a function of radial distance from the shower axis.

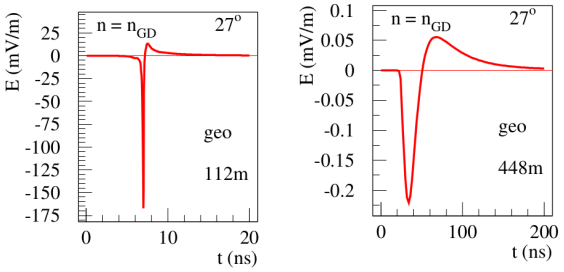

Figure 6: The geomagnetic contribution to the electric field for a 5×10^{17} eV, 27 degrees inclined shower observed at two different observer positions of $d = 112$ meters (left) and $d = 448$ meters (right) from the impact point of the shower. Figure taken from [14].

4 The electric field

Even though the currents become small close to the shower axis, the lateral weight function $w_1(r)$ increases strongly close to the core. As is shown in Fig. 3 the particle distribution close to the shower axis is very sharp (O(cm)). Therefore, emission is expected to occur at high-frequencies. This is also observed in Fig. 6, where the electric field is shown at $d = 112$ m from the shower axis, where Cherenkov emission is observed from close to the shower maximum, and at $d = 448$ m from the shower axis where Cherenkov effects have diminished. As expected, when Cherenkov effects occur in the emission, the electric field is observed in a very short time period and gets strongly enhanced leading a response at very high frequencies in the GHz region. Further away from the shower axis, these effects diminish and emission over longer time scales is observed at MHz frequencies.

5 Conclusions

An overview is given of the EVA code which incorporates Cherenkov effects in the radio emission from air showers. The EVA code consists out of three parts, there is the CX-MC-GEO package which performs a full Monte-Carlo CONEX simulation giving a histogrammed output of the charge and current distributions in the air shower. These distributions are fitted by the FITMC package to obtain smooth analytical functions which are used by the EVA radio emission calculation package to solve for the divergences due to Cherenkov emission. It is shown that close to the shower axis the particle distributions become very narrow leading to emission at high frequencies (GHz) when Cherenkov effects are observed. At larger distances these effects diminish giving emission at lower frequencies in the MHz regime. The EVA package is now publicly available and can be obtained by sending an e-mail to the authors.

References

[1] D. Ardouin, et al., CODALEMA Coll., Astropart. Phys. 26, (2006), 341
[2] D. Ardouin, CODALMA Coll., Astropart. Phys. 31, (2009), 192-200
[3] H. Falcke, et al., LOPES Coll., Nature 435, (2005), 313
[4] W. D. Apel, et al., LOPES Coll., Astropart. Phys. 26, (2006), 332
[5] S. Fliescher, Pierre Auger Coll., Nucl. Instr. and Meth. A 662, (2012), S124-S129
[6] A. Horneffer, et al., LOFAR CR-KSP, Nucl. Instr. and Meth. A 617, (2010), 482
[7] F. Schröder, et al., Proceedings of ARENA 2012, to be published, arXiv:1301.2555
[8] T. Huege, R. Ulrich, R. Engel, Astropart. Phys., 27, (2007), 392-405
[9] K.D. de Vries, A.M. van den Berg, O. Scholten, K. Werner, Astropart. Phys. 34, (2010), 267
[10] T. Huege, M. Ludwig, C. James, proceedings of ARENA 2012, to be published
[11] J. Alvarez-Muniz, W. R. Carvalho, Jr., E. Zas, Astropart. Phys. 35, (2012), 325-341
[12] V. Marin, B. Revenu, Astropart. Phys. 35, (2012), 733-741
[13] N.N. Kalmykov, A.A. Konstantinov, and R. Engel, Phys. At. Nucl. 73, (2010), 1191
[14] K. Werner, K.D. de Vries, O. Scholten, Astropart. Phys. 37, (2012), 5-16
[15] F.D. Kahn and I. Lerche, Proc. Royal Soc. London A289, (1966), 206
[16] G.A. Askaryan, Sov. Phys. JETP 14, (1962), 441; 21, (1965), 658
[17] T. Huege, et al., LOPES Coll., Nucl. Instr. and Meth. A 662, (2012), S72-S79
[18] H. Schoorlemmer for the Pierre Auger Collaboration, Proc. of ARENA 2010, Nucl. Instr. and Meth. A 662, (2012), S134-S137
[19] V. Marin for the CODALEMA Collaboration, Proc. of the 32nd ICRC 1, (2011), 291
[20] K.D. de Vries, A.M. van den Berg, O. Scholten, K. Werner, Phys.Rev.Lett. 107, (2011), 061101
[21] G. Bossard, et al., Phys. Rev. D 63, (2001), 054030
[22] T. Bergmann, et al., Astropart. Phys. 26, (2007), 420
[23] K.D. de Vries, O. Scholten, K. Werner, Astropart. Phys 45, (2013), 23-27
[24] K. Werner, O. Scholten, Astropart.Phys. 29, (2008), 393, arXiv:0712.2517 [astro-ph]
[25] O. Scholten and K. Werner, Nucl. Instr. and Meth. A 604, (2009), S24